ENERGY TRANSFER ANALYSIS FOR LARGE-SCALE UNSTEADINESS OF CYLINDER WAKE BASED ON TRIADIC ORTHOGONAL DECOMPOSITION

Yuto Nakamura
Department of Aerospace Engineering
Tohoku University
Sendai, 980-8579, Miyagi, Japan

Department of Aerospace Engineering
Nagoya University
Nagoya, 464-8601, Aichi, Japan
yuto.nakamura.t4@dc.tohoku.ac.jp

Shintaro Sato
Department of Aerospace Engineering
Tohoku University
Sendai, 980-8579, Miyagi, Japan
shintaro.sato.c3@tohoku.ac.jp

Naofumi Ohnishi
Department of Aerospace Engineering
Tohoku University
Sendai, 980-8579, Miyagi, Japan
naohnishi@tohoku.ac.jp

ABSTRACT

This study clarifies the energy-transfer mechanisms of low-frequency components embedded in Mode A of the cylinder wake using triadic orthogonal decomposition. To suppress the complexity promoted by the emergence of these low-frequency components, the computational spanwise domain is restricted to the most unstable wavelength of Mode A. Within this restricted domain, multiple peaks clearly appear at frequencies lower than the vortex-shedding frequency. These peaks interact with the Kármán vortex-shedding frequency f_K. The component of lowest-frequency f_b is associated with the well-known pumping phenomenon of the wake recirculation bubble. Application of triadic orthogonal decomposition reveals a cycle of energy transfer across the entire flow field, expressed as $f_K \to (f_K + f_b) \to f_b \to f_K \to \cdots$. Furthermore, visualization of the transfer distribution shows that this energy-transfer relationship is reversed in the near-cylinder region. These findings advance our understanding of the mechanisms that maintain low-frequency dynamics in cylinder wakes.

Introduction

Flows past bluff bodies exhibit a wide range of unsteady shear-flow phenomena that are of both fundamental and practical importance. The wake behind a circular cylinder has long served as a canonical configuration for investigating vortex dynamics in shear flows. Among its various features, the emergence of large-scale, low-frequency unsteadiness has attracted attention because it influenced the overall flow field (Berger *et al.*, 1990).

Previous studies have shown that such low-frequency components are closely linked to three-dimensional instabilities, especially Mode A, a well-known instability that emerges around a Reynolds number of 200 and manifests as three-dimensional vortex structures with a spanwise wavelength of about four times cylinder diameters (Williamson, 1996; Henderson & B., 1996). Figure 1 shows an isosurface of the Q-value, colored by the streamwise velocity component, obtained from the incompressible numerical simulation whose spanwise computational domain size is $3.9D$, where D represents cylinder diameter. Details of numerical methods are provided in (Nakamura *et al.*, 2026*a*,*b*). The Mode A dynamics are particularly sensitive to the computational domain size in the spanwise direction because the spanwise wavelength of Mode A is relatively larger than in high-Reynolds-number scenarios. When the spanwise extent of the domain is sufficiently large, the Mode A wake exhibits complex spectral characteristics with an abundance of low-frequency components, to the extent that no clear peaks can be distinguished. By contrast, when the spanwise domain size is restricted to be comparable to the spanwise wavelength whose growth rate is the largest at the two-dimensional flow state, distinct spectral peaks clearly emerge at low frequencies (Jiang *et al.*, 2017; Nakamura *et al.*, 2026*b*).

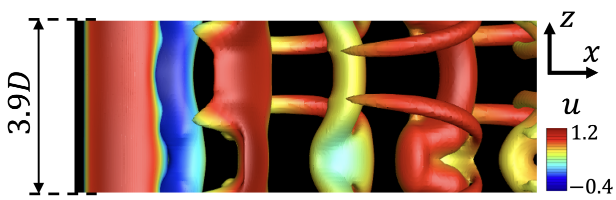

Figure 1. Isosurfaces of the Q-value at 0.1, colored by the streamwise (x-direction) velocity component at Reynolds number of 200.

Identification of these spectral peaks has further revealed that the low-frequency components interact nonlinearly with one another, and similar frequency components also exist in the large spanwise domain case. While previous observations suggest the existence of interaction, thereby complicating the overall wake dynamics, which is marked as quasi periodic state (Noack *et al.*, 1993; Henderson, 1997; Nakamura *et al.*, 2026*b*), the precise mechanisms of energy transfer between the dominant shedding and the low-frequency components remain insufficiently understood. To address this gap, we employ triadic orthogonal decomposition (TOD) (Yeung *et al.*, 2026, 2024), a recently developed framework that isolates nonlinear triadic interactions in stationary flow fields. TOD systematically identifies energy-transfer pathways and their spatial distributions among frequency components, thereby clarifying how the dominant Kármán vortex shedding mode interacts with low-frequency components.

Triadic Orhogonal Decomposition

The recipient–donor framework of the nonlinear term in momentum equations provides the foundation for quantifying nonlinear interactions among different frequency components (Phillips, 1960; Kraichnan, 1959; Nakamura *et al.*, 2025). The direction and magnitude of energy transfer between the donor frequency component $\hat{u}_l(x)$ and the recipient frequency component $\hat{u}_n(x)$ through the convection (catalyst) frequency component of $\hat{u}_l(x)$, where $\hat{\cdot}$ represents spectrum, is expressed as

$$E_{l\to n} = -\int \hat{u}_n^H \{(\hat{u}_{n-l}\cdot\nabla)\hat{u}_l\}\, dx = -\langle(\hat{u}_{n-l}\cdot\nabla)\hat{u}_l, \hat{u}_n\rangle, \quad (1)$$

where the superscript H denotes the Hermitian transpose of a vector defined in the three spatial directions (x,y,z). Here, $E_{l\to n}$ denotes the amount of energy transfer from $\hat{u}_l$ to $\hat{u}_n$, where a negative value indicates transfer in the opposite direction.

TOD (Yeung *et al.*, 2026, 2024) considers the optimal covariance for each donor-recipient pair, $\sigma(l,n)$, is given by the optimization problem

$$\sigma(l,n) = \underset{\psi_{l\to n},\varphi_n}{\operatorname{argmax}}\, \mathscr{E}\left\{-\frac{\langle(\hat{u}_{n-l}\cdot\nabla)\hat{u}_l, \psi_{l\to n}\rangle\langle\hat{u}_n,\varphi_n\rangle}{\|\varphi_n\|\|\psi_{l\to n}\|}\right\}, \quad (2)$$

where $\mathscr{E}$ represents the expected value that accounts for statistical fluctuations of the spectrum, and $\psi_{l\to n}$ and φ_n represent the convective and recipient modes, respectively. Note that this maximization problem reduces to the same formulation as SPOD (Lumley, 1967; Towne *et al.*, 2018; Schmidt & Colonius, 2020) when $\{(\hat{u}_{n-l}\cdot\nabla)\hat{u}_l\} \to \hat{u}_n$. In summary, TOD is a maximum covariance analysis (Storch & Zwiers, 1984) that maximizes the correlation between $\{(\hat{u}_{n-l}\cdot\nabla)\hat{u}_l\}$ and $\hat{u}_n(x)$.

The optimal energy transfer quantities from the $\hat{u}_l$ to the $\hat{u}_n$ frequency component is given by Real $\{\sigma(l,n)\langle\varphi_n, \psi_{l\to n}\rangle\}$. Since the transfer quantity is determined by the real part, it is sufficient to evaluate the expression for $f_n \geq 0$. Moreover, because the energy transfer quantities are defined through spatial integration, the local distribution of energy transfer can be inferred from the integrand:

$$T_{l\to n}(x) = \mathrm{Real}\left\{\sigma(l,n)\varphi_n^H(x)\psi_{l\to n}(x)\right\}. \quad (3)$$

The spatial distribution of $T_{l\to n}(x)$ is referred to as the transfer field. A positive value indicates energy transfer from $\hat{u}_l$ to $\hat{u}_n$, whereas a negative value indicates transfer in the opposite direction, from $\hat{u}_n$ to $\hat{u}_l$.

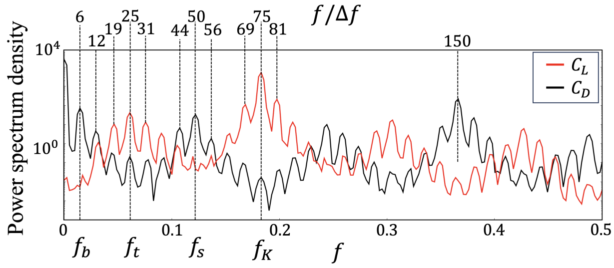

Figure 2. Power spectral density of lift and drag coefficients. The FFT was computed with a time window of $T = 409.6$, using a Hanning window, giving a frequency resolution of $\Delta f = 1/T = 2.44\times10^{-3}$.

Results

When the spanwise domain size is $3.9D$ in numerical simulation, the cylinder wake at Reynolds number 200 exhibits frequency components lower than the Kármán vortex shedding frequency (Nakamura *et al.*, 2026*b*). Figure 2 shows the power spectral density obtained by applying FFT to the time series of lift and drag coefficients, with frequency resolution of $\Delta f = 2.44\times10^{-3}$. The dominant peak appears in the lift coefficient and corresponds to the primary vortex-shedding frequency. This study denotes the largest nondimensional peak frequency of the lift coefficient as f_K (the Kármán vortex-shedding frequency). At higher frequencies, a spectral peak is observed at the harmonic $2f_K$ (with $f/\Delta f = 150$).

For frequencies lower than f_K, distinct peaks are observed in both the lift and drag coefficients. In particular, prominent peaks appear at $f/\Delta f = 25$ and $f/\Delta f = 50$, each peak exceeding the surrounding spectral peak levels. Within this spanwise domain size, the triadic relationship $25+50 = 75$ is satisfied. These frequencies are hereafter denoted as $f_t = 25\Delta f$ (third subharmonics) and $f_s = 50\Delta f$ (secandary-third subharmonics), respectively.

Focusing on the satellite peaks of f_t and f_s, their differences can be expressed as $f_t/\Delta f - 19 = 31 - f_t/\Delta f = f_s/\Delta f - 44 = 56 - f_s/\Delta f = 6$. These values coincide with the lowest nonzero peak frequency at $f/\Delta f = 6$. Thus, the $f/\Delta f = 6$ component interacts with other spectral peaks through their satellites. The previous study (Nakamura *et al.*, 2026*b*) has shown that this lowest frequency corresponds to the recursive expansion and contraction of the recirculation bubble in the cylinder wake, a phenomenon known as recirculation bubble pumping (Berger *et al.*, 1990). In this study, we define the corresponding frequency as $f_b = 6\Delta f$ (frequency of bubble pumping).

To investigate the interaction relationships associated with low-frequency components, we applied TOD to the entire flow field. Figure 3 presents a scatter plot of the energy budget, with donor frequency f_l on one axis and recipient frequency f_n on the other. Along the line $f_n = f_t$, positive energy transfer is observed at $f_l = f_K, 0$, and $-f_K$, indicating that the f_t-frequency component receives energy from these frequency elements. Similarly, along the line $f_n = f_s$, positive energy transfer is detected not only from $f_l = f_K, 0$, and $-f_K$, but also from $f_l = -f_t$. Considering the triadic relationship, this implies that the frequency f_s satisfies $f_s = -f_t + (f_s + f_t) = -f_t + f_K$.

Along the line $f_n = f_b$, the largest positive energy trans-

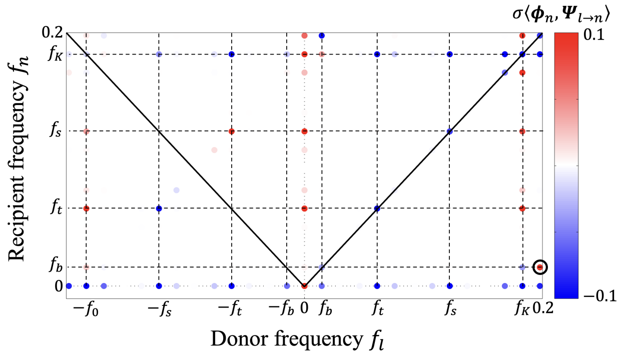

Figure 3. Scatter plots of modal energy budget. The frequencies f_K, f_s, f_t, and f_b are indicated in the figure by dashed lines.

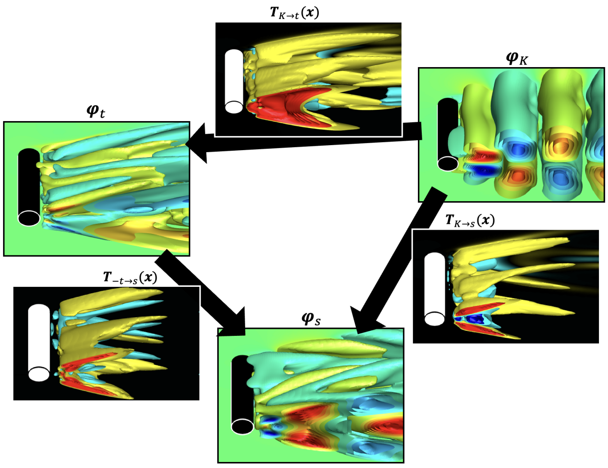

Figure 4. Summary of energy-transfer relationships among f_s, f_t, and f_K. All recipient modes are visualized using the real part of the streamwise velocity component. The arrows indicate the direction of energy transfer integrated over the spatial domain.

fer is observed from the satellite peak frequency $f_K + f_b$ (indicated by the black circle in the figure). This indicates that the f_b-frequency oscillation is maintained by a $(f_K + f_b)$-frequency component whose frequency is a slight shift of the vortex-shedding frequency f_K. Now, we refer to the $f_K + f_b$ frequency as f_K^+. Focusing on the f_K^+-frequency component, it is evident that a significant portion of energy is transferred from f_K. This interaction is governed by the relation $f_K + f_b = f_K^+$, suggesting that fluctuations in the vortex shedding frequency are induced by the pumping motion of the recirculation bubble. Numerous studies(Mantič-Lugo *et al.*, 2014; Barkley, 2006; Nakamura *et al.*, 2025) on flow around a cylinder suggested a correlation between the length of the recirculation region and the vortex shedding frequency. As the pumping motion of the recirculation bubble induces recursive variations in this length, the resulting energy transfer to frequency components slightly offset from the primary vortex shedding frequency aligns with previous findings.

Figure 4 summarizes the relationships among the frequency components from the perspective of energy transfer, together with the distributions of the recipient modes φ and transfer fields T. The arrows connecting each recipient mode $\varphi_{f_l}^{\mathrm{TOD}}$ indicate the direction of energy transfer, consistent with the energy transfer terms summarized in Fig. 3. The transfer fields overlaid on these arrows represent the spatial distribution of energy transfer, with the sign taken to be positive in the direction indicated by the arrows. The recipient modes φ_t and φ_s, where the subscripts t and s correspond to subscripts of frequencies, exhibit antisymmetric and symmetric distributions with respect to $y = 0$, respectively. The transfer fields $T_{K\to t}$ and $T_{K\to s}$ share the same asymmetric and symmetric properties as φ_t and φ_s. In addition, all transfer fields exhibit localized regions of large energy exchange at specific spanwise locations. These similarities suggest that f_t- and f_s-frequency components receive energy from Kármán vortices at specific spanwise locations.

A well-known phenomenon involving subharmonic components occurs during the onset of three-dimensionality in boundary layer transition, where energy is transferred from the primary-frequency component to the subharmonic component(Craik, 1971; Kim *et al.*, 2021). In this scenario, the subharmonic component typically appears at exactly half the primary frequency. Thus, the energy transfer from the primary-frequency component to the subharmonic component is mediated by the subharmonic component itself; consequently, its amplification triggers further energy transfer, eventually leading to a three-dimensional breakdown. Specifically, this represents a difference-interaction characterized by the triadic relation $f_p - (f_p/2) = f_p/2$, where f_p denotes the primary frequency. While the energy distribution for the subharmonic components in the present study also originates from a difference-interaction, it deviates from the boundary layer transition scenario in that the frequencies are not exact half-harmonics. Consequently, even when a difference-interaction occurs, the energy is dispersed across multiple subharmonic frequencies, f_t and f_s. This dispersion likely prevents the rapid energy amplification typically observed in exact subharmonic resonance.

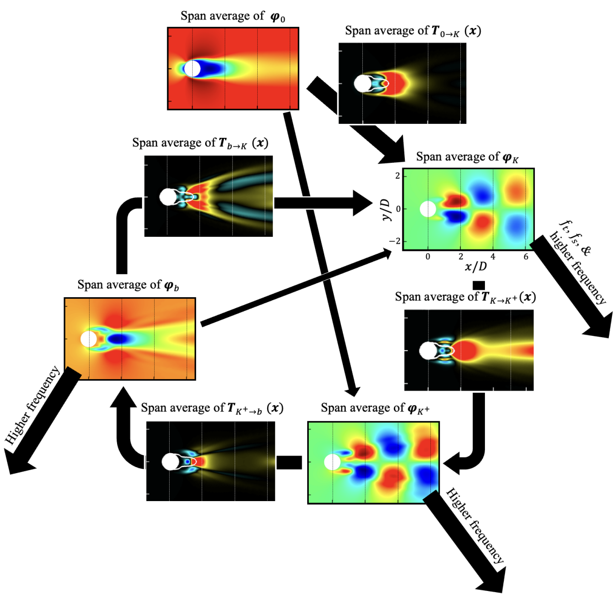

Figure 5. Summary of energy-transfer relationships among f_K, f_b, and f_K^+. All spatial distributions are averaged over the spanwise direction.

Figure 5 shows the relationships among the f_b and f_K-frequency components with the distributions of the recipient modes φ and transfer fields T. Considering f_K, f_b, and the satellite peak frequency $f_K^+ (= f_K + f_b)$, a cycle of energy transfer is identified, following the sequence $f_K \to f_K^+ \to f_b \to f_K \cdots$. It should be noted that the magnitudes of transfer quantities are not identical, so the cycle does not form a perfectly closed cycle. The transfer fields $T_{K \to K^+}$, $T_{K^+ \to b}$, and $T_{b \to K}$ show that negative transfer arises in all cases near the cylinder. This suggests that the direction of the cycle indicated by the arrows is reversed in the near-wake region. Such reversals of the energy-transfer cycle occur approximately along the boundary of the wake recirculation bubble, implying that the direction of energy transfer changes with the orientation of the streamwise velocity.

Conclusion

The present analysis revealed that low-frequency components in the cylinder wake at a Reynolds number of 200 interact with the primary vortex-shedding frequency, its satellites, and the frequency of recirculation bubble pumping. The application of TOD clarified the energy pathways: the f_t and f_s components receive energy primarily from f_K and its satellites. These energy transfer pathways are driven by nonlinear interactions mediated by another low-frequency component. In contrast, the bubble-pumping oscillation is maintained through interactions with $f_K^+ (= f_K + f_b)$. These transfers form a cyclic relationship, $f_K \to f_K^+ \to f_b \to f_K$, whose direction reverses in the near-wake region around the recirculation bubble. This reversal highlights the critical role of wake dynamics in governing the maintenance of low-frequency wake unsteadiness.

REFERENCES

Barkley, D. 2006 Linear analysis of the cylinder wake mean flow. *Europhysics Letters* **75** (5), 750.

Berger, E., Scholz, D. & Schumm, M. 1990 Coherent vortex structures in thewake of a sphere and a circular disk at rest and under forced vibrations. *Journal of Fluids and Structures* **4** (3), 231–257.

Craik, A. D. D. 1971 Non-linear resonant instability in boundary layers. *Journal of Fluid Mechanics* **50** (2), 393–413.

Henderson, R. D. 1997 Nonlinear dynamics and pattern formation in turbulent wake transition. *Journal of Fluid Mechanics* **352**, 65–112.

Henderson, R. D. & B., Dwight 1996 Secondary instability in the wake of a circular cylinder. *Physics of Fluids* **8** (6), 1683–1685.

Jiang, H., Cheng, L. & An, H. 2017 On numerical aspects of simulating flow past a circular cylinder. *International Journal for Numerical Methods in Fluids* **85** (2), 113–132.

Kim, M., Kim, S., Lim, J., Lin, R.-S., Jee, S. & Park, D. 2021 Effects of phase difference between instability modes on boundary-layer transition. *Journal of Fluid Mechanics* **927**, A14.

Kraichnan, R. H. 1959 The structure of isotropic turbulence at very high Reynolds numbers. *Journal of Fluid Mechanics* **5** (4), 497–543.

Lumley, J. L. 1967 *The structure of inhomogeneous turbulent flows. In Atmospheric Turbulence and Radio Wave Propagation*, a. m. yaglom & v. i. tatarski edn., pp. 166–178. Nauka.

Mantič-Lugo, V., Arratia, C. & Gallaire, F. 2014 Self-consistent mean flow description of the nonlinear saturation of the vortex shedding in the cylinder wake. *Physical Review Letters* **113** (8).

Nakamura, Y., Kuroda, Y., Sato, S. & Ohnishi, N. 2025 Energy transfer and budget analysis for transient process with operator-driven reduced-order model. *arXiv preprint arXiv:2503.20204* .

Nakamura, Y., Sato, S. & Ohnishi, N. 2026*a* Improvement of reduced-order model for two-dimensional cylinder flow based on global proper orthogonal decomposition in terms of robustness and computational speed. *Journal of Fluids Engineering* pp. 1–29.

Nakamura, Y., Sato, S. & Ohnishi, N. 2026*b* Uncovering triadic interaction relationships latent in mode a for the wake of a circular cylinder. *Journal of Fluid Mechanics* **1030**, A12.

Noack, B. R., König, M. & Eckelmann, H. 1993 Three-dimensional stability analysis of the periodic flow around a circular cylinder. *Physics of Fluids* **5** (6), 1279–1281.

Phillips, O. M. 1960 On the dynamics of unsteady gravity waves of finite amplitude part 1. the elementary interactions. *Journal of Fluid Mechanics* **9** (2), 193–217.

Schmidt, O. T. & Colonius, T. 2020 Guide to spectral proper orthogonal decomposition. *AIAA Journal* **58** (3), 1023–1033.

Storch, H. von & Zwiers, F. W. 1984 *Statistical Analysis in Climate Research*. Cambridge University Press.

Towne, A., Schmidt, O. T. & Colonius, T. 2018 Spectral proper orthogonal decomposition and its relationship to dynamic mode decomposition and resolvent analysis. *Journal of Fluid Mechanics* **847**, 821–867.

Williamson, C. H. K. 1996 Mode A secondary instability in wake transition. *Physics of Fluids* **8** (6), 1680–1682.

Yeung, B., Chu, T. & Schmidt, O. T. 2024 Revealing structure and symmetry of nonlinearity in natural and engineering flows. *arXiv preprint arXiv:2411.12057* .

Yeung, B., Chu, T. & Schmidt, O. T. 2026 Triadic orthogonal decomposition reveals nonlinearity in fluid flows. *Journal of Fluid Mechanics* **1031**, A34.